In: 2023 AIAA Aviation and Aeronautics Forum and Exposition (AIAA AVIATION Forum),
12-16 June 2023, San Diego, USA
DOI:10.2514/6.2023-3284

Control of Flow Separation in a High-speed Compressor Cascade through Acoustic Excitation

Seyfettin Coskun*, David John Rajendran † and Vassilios Pachidis‡
Cranfield University, Cranfield, Bedfordshire, MK43 0AL, UK

Marko Bacic§
Rolls-Royce plc., Derby, Derbyshire, DE21 8BJ, UK

The use of acoustic excitation for controlling flow separation in a NACA65-K48 linear compressor cascade operating at aircraft engine representative $Ma = 0.67$ and $Re_c = 560\,x10^3$ is investigated numerically. Improved Delayed Detached Eddy Simulation (IDDES) is used for numerical simulations. The linear compressor cascade passage under investigation is subject to severe secondary flows that are the fundamental loss mechanisms in axial compressors. Secondary flows such as corner separation cover a significant portion of the blade height of the linear compressor cascade (LCC) because of its low aspect ratio. These losses result in passage blockage which results in performance degradation. In the current study, the effect of external acoustic excitation on flow separation characteristics in the compressor passage is examined. The effectiveness of acoustic excitation is investigated for two main excitation parameters: excitation frequency and amplitude. The dominant frequencies in the uncontrolled flow frequency spectra are used as the initial excitation frequencies whilst a range of excitation amplitudes are considered. It has been observed that when the acoustic excitation is applied with a frequency in the range of the most dominant frequency in the uncontrolled flow and an excitation amplitude above a threshold amplitude, the flow field can be modulated substantially to recover the cascade performance.

I. Nomenclature

c	=	chord length
C_{ax}	=	axial chord length
Δt	=	numerical time step
f_0	=	fundamental frequency of the most amplified disturbances within the shear layer
f_{exc}	=	acoustic excitation frequency
h	=	blade height
i	=	incidence angle
t	=	pitch length
ν	=	kinematic viscosity of air
Re_c	=	Reynolds number based on chord length, $U_\infty c/\nu$
St	=	Strouhal number, fc/U_∞
τ	=	$t(U_\infty/c)$, convective time
ADP	=	Aerodynamic Design Point
EW	=	Endwall
IDDES	=	Improved Delayed Detached-Eddy Simulation
LCC	=	Linear Compressor Cascade
SPL	=	Sound Pressure Level, dB
ζ	=	Total pressure loss coefficient, $\frac{P_{t,in}-P_t}{P_{t,in}-P_{in}}$

*PhD Researcher, Rolls-Royce UTC, Centre for Propulsion and Thermal Power Engineering, e-mail: seyfettin.coskun@cranfield.ac.uk.
†Lecturer, Rolls-Royce UTC, Centre for Propulsion and Thermal Power Engineering, e-mail: D.Rajendran@cranfield.ac.uk.
‡Professor, Rolls-Royce UTC, Centre for Propulsion and Thermal Power Engineering, e-mail: v.pachidis@cranfield.ac.uk.
§PhD, Rolls-Royce plc.

II. Introduction

Secondary flows such as the cross flow between the pressure and suction surfaces of consecutive blades and corner separation at the junction of cascade endwall and blade suction surface result in passage blockage and high levels of total pressure losses. Secondary flows are fundamental loss mechanisms in axial flow compressors due to their unsteady and three-dimensional nature [1, 2]. The current trend in aerodynamic design of axial compressors involve reduction on the number of blades and stages, which results in an increase in blade aerodynamic loading. The increase in aerodynamic loading results in higher adverse pressure gradients across a stage, which essentially undermines the aerodynamic stability of axial compressors and imposes limiting factors on the compressor performance and operability [3, 4]. Therefore, any improvement on this flow that is highly susceptible to separation and generation of severe losses can provide substantial performance and operability enhancements.

Acoustic excitation as a means of flow control has been successfully demonstrated in low to moderate subsonic flows over isolated aerofoils [5–10] and low-pressure turbines [11–14]. However, in high-subsonic/transonic compressor cascades that are dominated by secondary flows, the use of acoustic excitation for flow control has not yet been investigated thoroughly. Therefore, control of these flow mechanisms can provide considerable improvements on the design of axial compressors. Acoustic excitation can be applied in the form of both internal and external excitation, depending on the location of sound source. In external acoustic excitation, a sound source is located away from the geometry of interest whereas sound source is located inside the boundary layer, usually on or underneath a surface of geometry in internal excitation. The current work focuses on external acoustic excitation of a compressor cascade flow and internal acoustic excitation will be a part of the future work.

Massive flow separations are encountered in low aspect ratio LCC's including operations at aerodynamic design points. A significant portion of the blade span is dominated by the corner separation, which results in severe losses in the cascade. Therefore, accurate modelling of the uncontrolled flow field including secondary flows plays a critical role in application of acoustic excitation as the effective excitation frequencies are estimated from the uncontrolled flow. Furthermore, unsteady and three-dimensional nature of the uncontrolled flow and modelling of acoustic wave and flow interactions require a sophisticated turbulence modelling approach as observed in several previous studies. The accurate prediction of the flow separation including the secondary flows in LCC passages requires use of scale resolving turbulence models such as Large Eddy Simulation(LES). However, the computational cost of an LES is prohibitive for high Reynolds number flows and hybrid methods which combine advantages of both RANS and LES methods, can be suited to such flows. Detached-Eddy Simulation (DES) is one of the hybrid RANS-LES methods that takes advantage of the RANS modelling in near-wall regions and LES elsewhere with a lower computational requirement compared to a classical LES [16]. Improved Delayed Detached-Eddy Simulation (IDDES) is an improved version of DES resolving log-layer mismatch, as well as modelled stress depletion encountered in a classical DES [17]. Therefore, it is anticipated that IDDES provides the required accuracy with a relatively reasonable computational cost for the purposes of the current work.

The motivation of this work is to investigate the effect of acoustic excitation on flow loss mechanisms on a linear compressor cascade at transonic speeds. This work is based on a computational approach by use of IDDES for modelling the flow in the engine representative NACA65-K48 linear compressor cascade passage operating at $Ma = 0.67$ and $Re_c = 560\,x10^3$. The uncontrolled flow is analysed by a $k-\omega$ SST based IDDES model. The investigations include computational model validation, detailed examination of the effect of acoustic excitation on the flow separation and parametric studies on the effects of acoustic excitation frequency and amplitude.

III. Computational Setup and Methodology

A. Improved Delayed Detached Eddy Simulation (IDDES)

IDDES model is based on two-equation $k-\omega$ SST, with the following modifications to k and ω equations:

$$\frac{\partial(\rho k)}{\partial t} + \frac{\partial(\rho u_j k)}{\partial x_j} = \tau_{ij}\frac{\partial u_i}{\partial x_j} + \frac{\partial}{\partial x_j}\left[(\mu + \sigma_k \mu_t)\frac{\partial k}{\partial x_j}\right] - C_\mu \rho \omega k l_{IDDES} \tag{1}$$

$$\frac{\partial(\rho \omega)}{\partial t} + \frac{\partial(\rho u_j \omega)}{\partial x_j} = \frac{\gamma}{\nu_t}\tau_{ij}\frac{\partial u_i}{\partial x_j} - \beta \rho \omega^2 + \frac{\partial}{\partial x_j}\left[(\mu + \sigma_\omega \mu_t)\frac{\partial \omega}{\partial x_j}\right] + 2(1-F_1)\frac{\rho \sigma_{\omega 2}}{\omega}\frac{\partial k}{\partial x_j}\frac{\partial \omega}{\partial x_j} \tag{2}$$

where ρ is density, k is turbulent kinetic energy (TKE), ω is specific dissipation, x_i represents spatial coordinates, t is time, μ is laminar viscosity, μ_t is turbulent eddy viscosity and l_{IDDES} is IDDES length scale given as;

$$l_{IDDES} = \tilde{f_d}(1 + f_e)l_{RANS} + (1 - \tilde{f_d})l_{LES} \tag{3}$$

$$\begin{aligned} l_{RANS} &= \frac{\sqrt{k}}{C_\mu k} \\ l_{LES} &= C_{DES}\Delta \\ C_{DES} &= C_{DES1}F_1 + C_{DES2}(1 - F_1) \end{aligned} \tag{4}$$

where l_{IDDES}, l_{RANS} and l_{LES} are IDDES, RANS and LES length scales, respectively. $C_{DES1} = 0.78$ and $C_{DES2} = 0.61$ are model constants and F_1 is a blending function.

The LES length scale is given by:

$$\Delta = min\left\{C_\omega\ max[d_\omega, h_{max}], h_{max}\right\} \tag{5}$$

where h_{max} is the cell maximum edge length and d_ω is the distance from the cell to the wall. $\tilde{f_d}$ in Eqn. 3 is an empirical blending function computed as:

$$\begin{aligned} \tilde{f_d} &= max\left\{(1 - f_{dt}), f_b\right\} \\ f_{dt} &= 1 - tanh[(C_{dt1} \cdot r_{dt})^{C_{dt2}}] \\ r_{dt} &= \frac{\nu_t}{\kappa^2 {d_\omega}^2 \sqrt{0.5(S^2\Omega^2)}} \\ f_b &= min\left\{2exp(-9\alpha^2), 1.0\right\} \\ \alpha &= 0.25 - d_\omega/h_{max} \end{aligned} \tag{6}$$

where κ is Karman constant, S is strain rate tensor magnitude and Ω is vorticity tensor magnitude. Further details can be found in Gritskevich [18] and Menter [19].

B. Computational Approach

High-speed linear compressor cascade NACA65-K48 is investigated numerically for flow separation control through external acoustic excitation. The cascade is composed of 5 linearly arranged consecutive blades with NACA65 profile distribution over a 48° circular arc. Cascade design inlet Mach number is $Ma = 0.67$ and Reynolds number based on blade chord length is $Re_c = 560\ x10^3$. All the simulations are based on $k - \omega$ SST based IDDES model. LCC under investigation is composed of low aspect ratio blades, i.e., $h/c = 1$, that results in significant secondary flow mechanisms in the passage flow due to blade-endwall interactions covering a considerable portion of the blade height. Design inflow angle with respect to vertical axis is $\beta_1 = 132°$ with a flow turning of $\Delta\beta = 42°$. Cascade design parameters and operating conditions are provided in Table 1.

Table 1 NACA65-K48 linear compressor cascade design parameters and operating conditions.

Inlet Mach Number	Ma_1	0.67	[−]
Inflow Angle	β_1	132	[°]
Flow Turning	$\Delta\beta$	42	[°]
Stagger Angle	β_s	112.5	[°]
Chord Length	c	40	$[mm]$
Solidity	t/c	0.55	[−]
Aspect Ratio	h/c	1	[−]
Incoming Endwall Boundary Layer Thickness	$\delta_{in,EW}$	4.0	$[mm]$

The computational geometry and grid along with how sound waves are introduced into the computational model are shown in Fig. 1. As the geometry is spanwise symmetric, half blade height is used in the computational work for the sake of computational efficiency with use of symmetry boundary conditions. The computational domain extends $0.8C_{ax}$ upstream of the blade leading edge and $2.5C_{ax}$ downstream from the trailing edge. Hexahedral O-C-H grid topology is used for computational grid generation. Numerical computations are carried out in ANSYS-Fluent, which is a cell-centred finite volume flow solver. A fully implicit pressure-based solver is utilized. Second-order numerical spatial discretization is used for the pressure, momentum and energy while Green-Gauss Node-Based spatial discretization is used for gradients and derivatives. Second-order implicit Newtonian dual-time stepping method is used for transient formulations with 15 pseudo sub-iterations per time advancement for solution of mean flow and turbulent quantities. Steady $k-\omega$ SST based RANS computations are used as precursor to transient $k-\omega$ SST IDDES model. Total pressure boundary condition is used at the computational domain inlet with a boundary layer distribution to provide the boundary layer thickness $\delta_{in,EW} = 4mm$ over the endwall at the inlet to match the experimental conditions [20]. Outlet static pressure is specified accordingly to satisfy the inlet Mach number, $Ma_1 = 0.67$. For the endwall and blade surfaces, no-slip adiabatic wall boundary conditions are applied. A single passage of the linear cascade is modelled with the use of periodic boundary conditions that account for the flow interactions between consecutive blades.

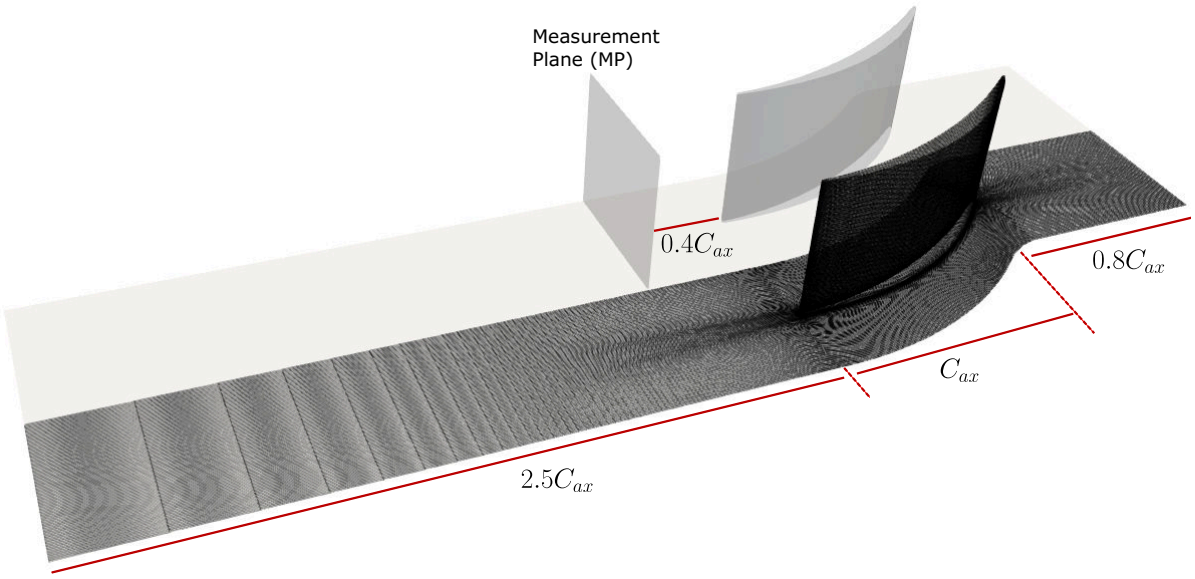

Fig. 1 Computational domain for half-span blade.

C. Acoustic Excitation Modelling

Generation of sound waves in the computational domain is implemented by the use of transient pressure inlet boundary conditions at the inlet boundary of the computational domain. The objective of the current work is the investigation of the effects of external acoustic excitation where sound source is located away from the geometry of interest. Monochromatic planar sound waves are used to generate acoustic disturbances on instantaneous freestream variables. Transient pressure inlet boundary condition is defined by:

$$P_t = P_{t,\infty}\left(1 + A_m e^{i(kx_i - \omega t)}\right)$$

$$T_t = T_{t,\infty}\left(1 + A_m \frac{\gamma - 1}{\gamma} e^{i(kx_i - \omega t)}\right)$$

where $P_{t,\infty}$ and $T_{t,\infty}$ are the inlet total pressure and temperature, respectively, in the absence of sound waves, A_m is excitation amplitude in percentage of $P_{t,\infty}$, $k = \sqrt{k_x^2 + k_y^2 + k_z^2} = \omega/c_0$ the wave number of planar waves and $\omega = 2\pi f_{exc}$ the circular frequency, f_{exc} excitation frequency and c_0 the speed of sound.

At the outlet boundary, non-reflecting boundary condition (NRBC) is used to remedy the spurious reflections back into the computational domain from the static pressure outlet BC used, which is highly reflective and may produce non-physical perturbations in the flow and hence reduce the order of accuracy [21, 22]. NRBC used here is based on characteristic wave reflections derived from Euler equations [23] to ensure transfer of sound waves out of the domain.

D. Validation

IDDES is used in the present work due to its promising capabilities in separated flows. Time-averaged local total pressure loss coefficient, ζ, given by Eqn. 7, distribution at the measurement plane (MP) located 40% axial chord length C_{ax} downstream of the blade trailing edge is used to compute the mass-flow averaged pitchwise total pressure loss coefficient distribution ζ_t according to Eqn. 8.

$$\zeta(y,z) = \frac{P_{01} - P_0(y,z)}{P_{01} - P_1} \tag{7}$$

$$\zeta_t = \iint_{MP} \zeta(y,z)\, dy \tag{8}$$

Comparison of IDDES prediction to experimental data [20] in Fig. 2 shows that current numerical approach predicts the total pressure loss downstream of the LCC passage in close agreement with the experimental data although IDDES model slightly overpredicts the total pressure loss for the core of corner separation. However, the level of accuracy of the computational approach is sufficient for the purposes of the current work. Therefore, IDDES is employed for the rest of the current work.

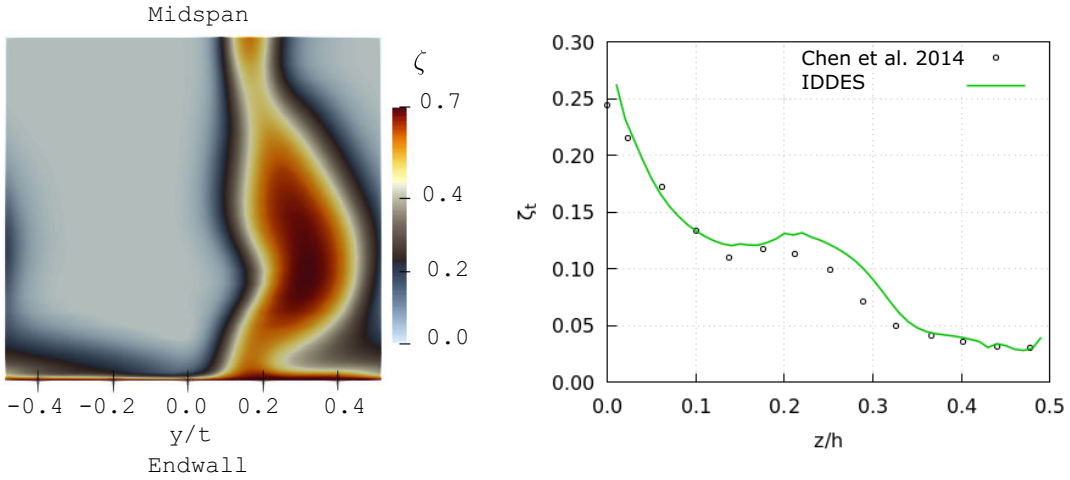

Fig. 2 Local total pressure loss coefficient distribution at MP (left) and mass flow averaged pitchwise distribution of total pressure loss coefficient (right).

Turbulent kinetic energy spectrum at the origin of corner separation shown in Fig. 3 reveals three distinct frequency peaks corresponding to St_c = 1.36, 2.18 and 2.72 in terms of the chord-based Strouhal number. These frequency peaks are taken as the excitation frequencies as it was shown in previous research that the fundamental frequencies of the baseline flow are the most effective frequencies for acoustic excitation [6–8, 10].

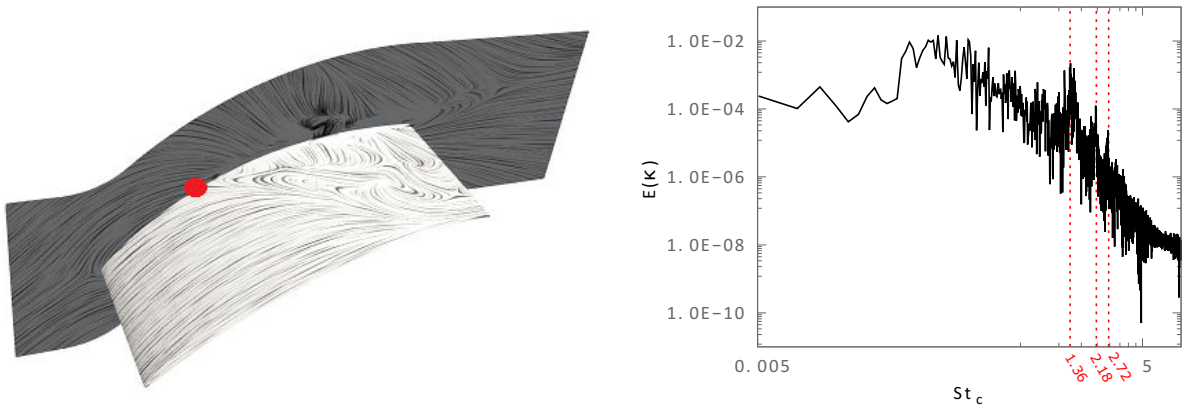

Fig. 3 Surface flow topology and the monitor location (left) and turbulent kinetic energy spectrum at the onset of corner flow separation (right).

IV. Results & Discussion

The effects of external acoustic excitation on flow separation in a linear compressor cascade operating at aerodynamic design point are discussed in the current work in the following manner:

- A frequency sensitivity study is carried out for identification of the effective acoustic excitation frequencies at a constant excitation amplitude. The modal frequencies obtained from the baseline flow, St_c = 1.36, 2.18 and 2.72, are used for identification of the effective frequencies.

- Upon obtaining the most effective frequency, a parametric study is conducted for excitation amplitude effect for sound pressures $131dB \leq SPL \leq 151dB$. Relatively higher excitation amplitudes are included for illustration of the sound wave amplitude effects.

First, a detailed analysis for the most effective acoustic excitation parameters is provided for illustration of the effects of acoustic excitation on flow field, the physics behind the sound waves and flow interactions and the effects of acoustic excitation on cascade performance. Thereafter, parametric studies on the excitation frequency and amplitude are discussed.

A. Effect of Acoustic Excitation

The effect of acoustic excitation on the uncontrolled flow is provided in this section for the most effective excitation parameters obtained in this study corresponding to excitation with St_c = 2.72 and SPL = 145dB. The effect of acoustic excitation is illustrated in Fig. 4 in terms of normalised root-mean-square error (RMSE) velocity contours at four spanwise planes at z/h = 0.125, 0.25, 0.375 and 0.49. It should be noted that z/h = 0.49 plane is selected for investigation of the midspan region to eliminate the effects of symmetry boundary condition used to reduce the spanwise extent of the domain as the midspan of the blade corresponds to the boundary of the computational domain. In all the planes shown, an increase in RMSE velocity is observed around the trailing edge region of the blade and downstream in the wake of the blade. This implies a rise in the turbulence levels by definition and hence an enhancement on the turbulent mixing downstream in the wake of the blade. The highest effect of acoustic excitation is observed around the midspan of the blade, i.e., z/h = 0.49, such that the location of the local maximum RMSE value is observed closer to the passage exit. Although no considerable change is observed in RMSE velocity in the vicinity of the blade suction surface where the corner separation takes place, the main effect of acoustic excitation is observed downstream of the trailing edge. Therefore, it is anticipated that external acoustic excitation does not result in a significant change in the evolution of corner flow separation topology whilst vortex shedding characteristics can be changed due to increased turbulent mixing at the wake of the cascade.

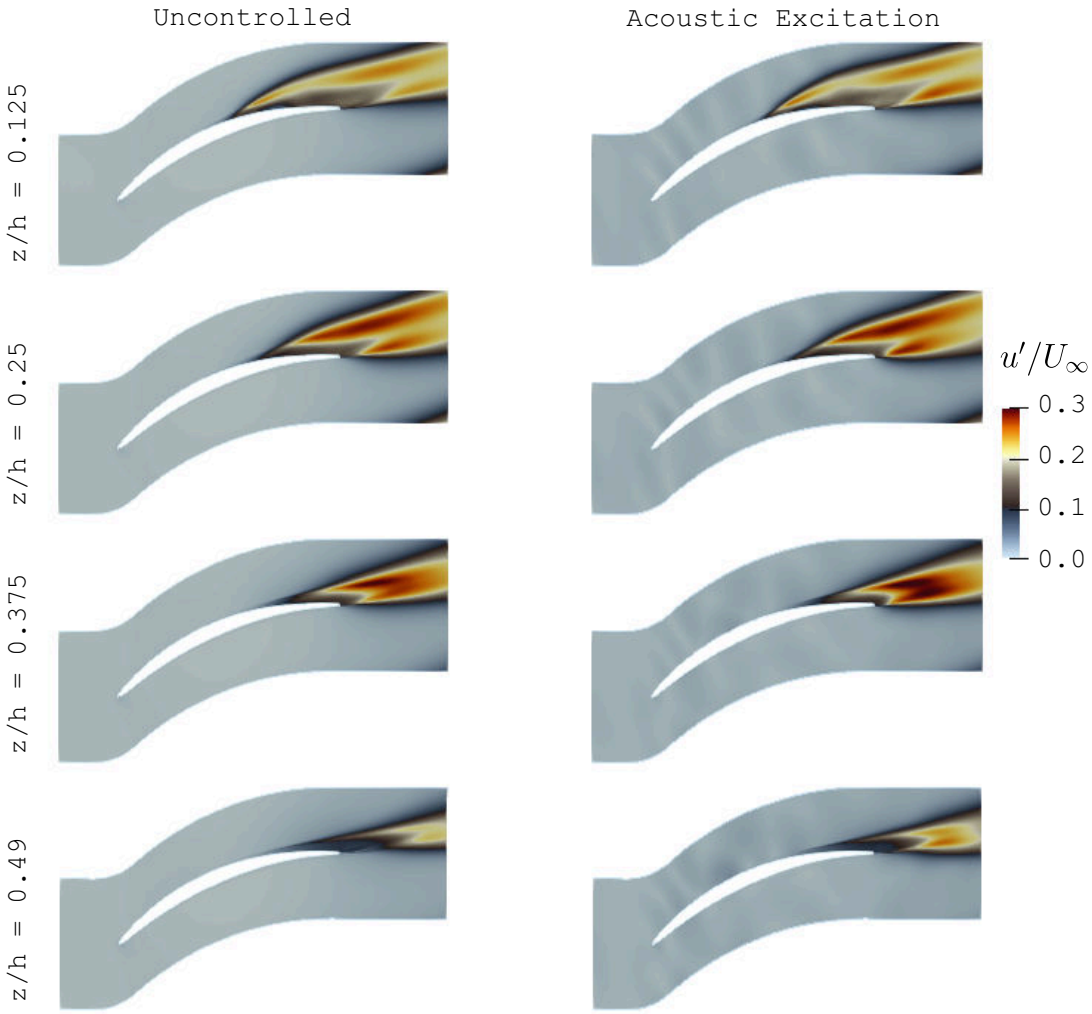

Fig. 4 Normalised RMSE velocity contours comparison for uncontrolled and excited flows at spanwise planes.

Instantaneous spanwise vorticity contours are compared in Fig. 5. Spanwise vorticity Ω_z is normalised by the blade chord length and the free stream velocity, $\Omega_z^* = \Omega_z * c/U_\infty$. In the uncontrolled flow, the signature of the corner flow separation can be seen in the nearby planes of the cascade endwall, i.e., from $z/h = 0.125$, in the form of a shear layer that separates from the blade suction surface and eventually breaks down. In the outer planes towards the midsection of the passage, shear layer gets closer to the blade suction surface with an accompanying delay in the location of shear layer break down. With the application of acoustic excitation, an earlier break down of the shear layer is observed at all the spanwise planes shown whilst the effect of acoustic excitation becomes more pronounced towards the passage midsection. At $z/h = 0.49$, shear layer breakdown takes place considerably upstream compared to the uncontrolled flow resulting in a rise in the coherence of vortical structures as shown in the figure. The increased coherence of the vortices improves the momentum transfer across the separated shear layer. Corresponding three-dimensional view of the vorticity distribution around the LCC blade shown in Fig. 6 demonstrates the change in the location of shear layer breakdown in the presence of acoustic excitation.

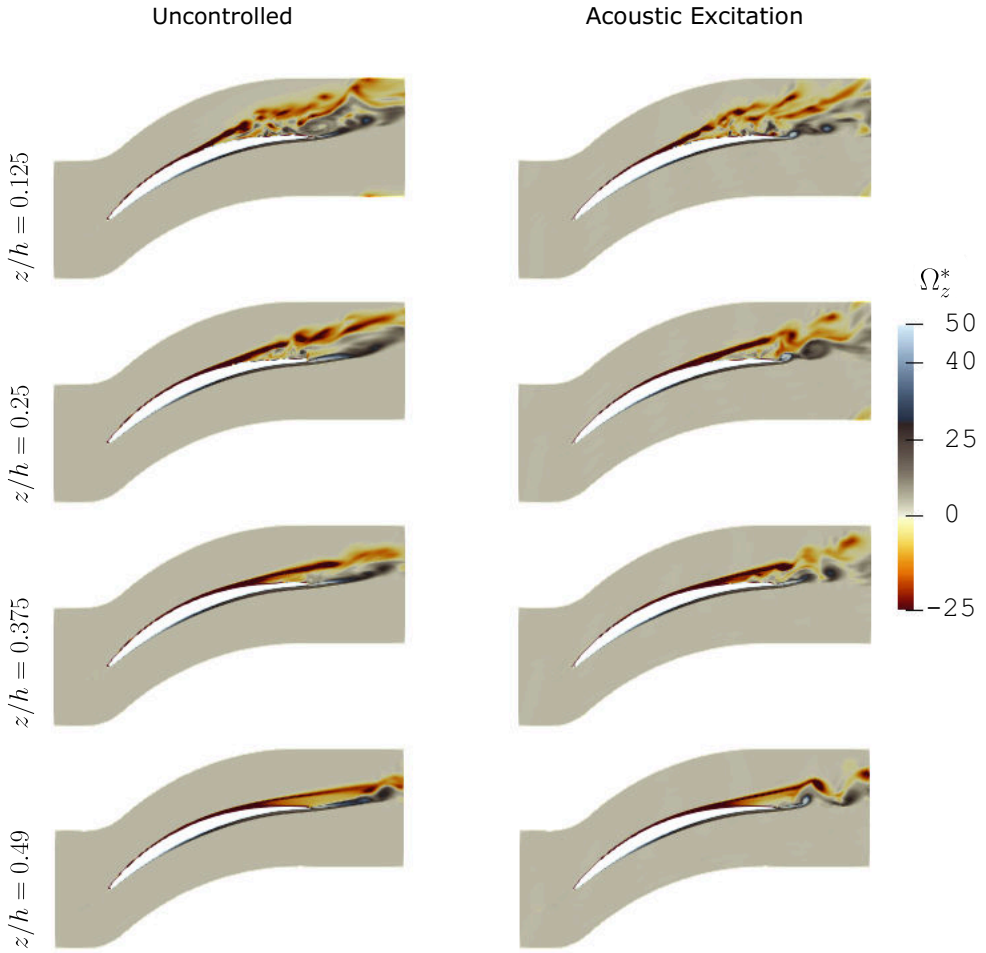

Fig. 5 Normalised spanwise vorticity Ω_z^* contours at spanwise planes.

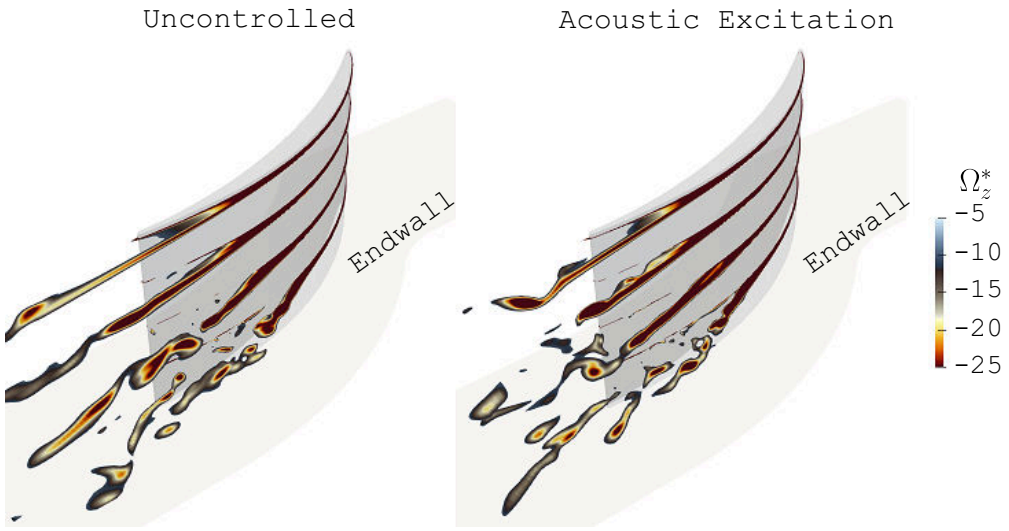

Fig. 6 3D view of Ω_z^* at spanwise stations.

The turbulent kinetic energy spectra at the monitor location in Fig. 3 are compared for uncontrolled and acoustically excited flows in Fig. 7. A better defined and energized frequency peak appears at the frequency of excitation, f_{exc} which corresponds to $St_c = 2.72$, in the excited flow. In acoustically excited flow, modal frequencies appear at the harmonic frequencies of acoustic excitation frequency for the 1^{st} and 2^{nd} harmonics that indicates locking of the excitation frequency to the fundamental frequency of the uncontrolled flow. This process results in an earlier transition to turbulence in the excited flow compared the uncontrolled flow with an enhanced energy spectrum characteristics of a turbulent flow. The turbulent kinetic energy cascade is also improved when the flow through the cascade is excited by sound waves. The improvement on the energy transfer from higher length scale eddies to smaller scales results in enhanced energy transfer from larger scale eddies to smaller ones, improving the improved energy cascade promotes generation of smaller length scale and higher frequency eddies in the excited flow. Moreover, the energy transfer across the separated shear layer to the near-wall low momentum flow within the corner separation is improved.

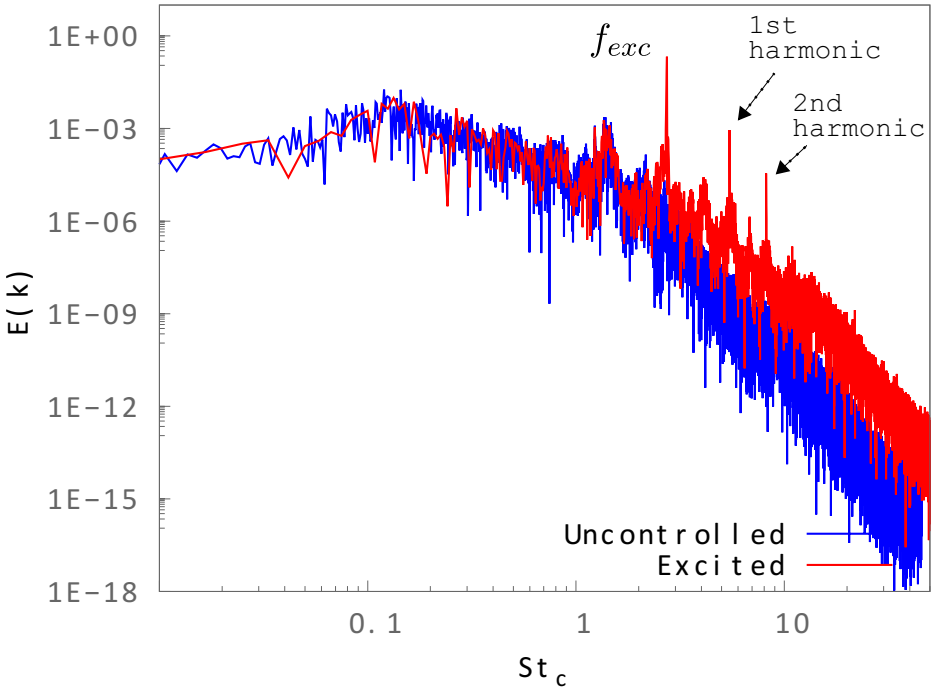

Fig. 7 The effect of acoustic excitation on turbulent kinetic energy spectrum at the onset of corner flow separation through the LCC passage.

Iso-surfaces of Q-criterion coloured by the normalised spanwise vorticity shown in Fig. 8 reveal the the change in vortex shedding characteristics of the cascade with application of acoustic excitation. Streamwise evolution of the corner separation starts from $x/c \approx 0.4c$ in the uncontrolled flow. With application of acoustic excitation, the vortical structures start to elongate in the spanwise direction of the blade although no reasonable change is observed at the origin of corner flow separation. Consequently, due to this vortex stretching, the corner vortex gets weaker with the application of acoustic excitation. As a result, a reduction in the wake velocity deficit is observed in the spanwise planes at MP as illustrated in Fig. 9. The effect of acoustic excitation becomes more pronounced towards the midspan of the blade such that $\Delta U/U_{ex} \approx 15\%$ reduction in the velocity deficit is gained. This is in agreement with RMSE velocity and vorticity analyses shown in Fig. 4 & 5.

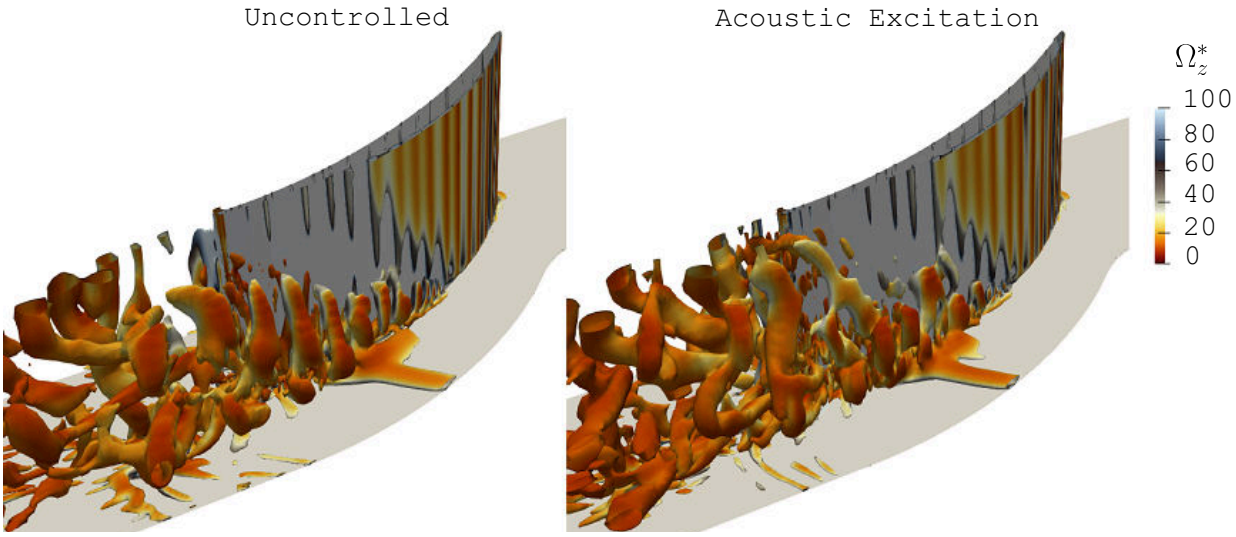

Fig. 8 Iso-surfaces of Q-criterion at $Q = 10^9$ coloured by Ω_z^*.

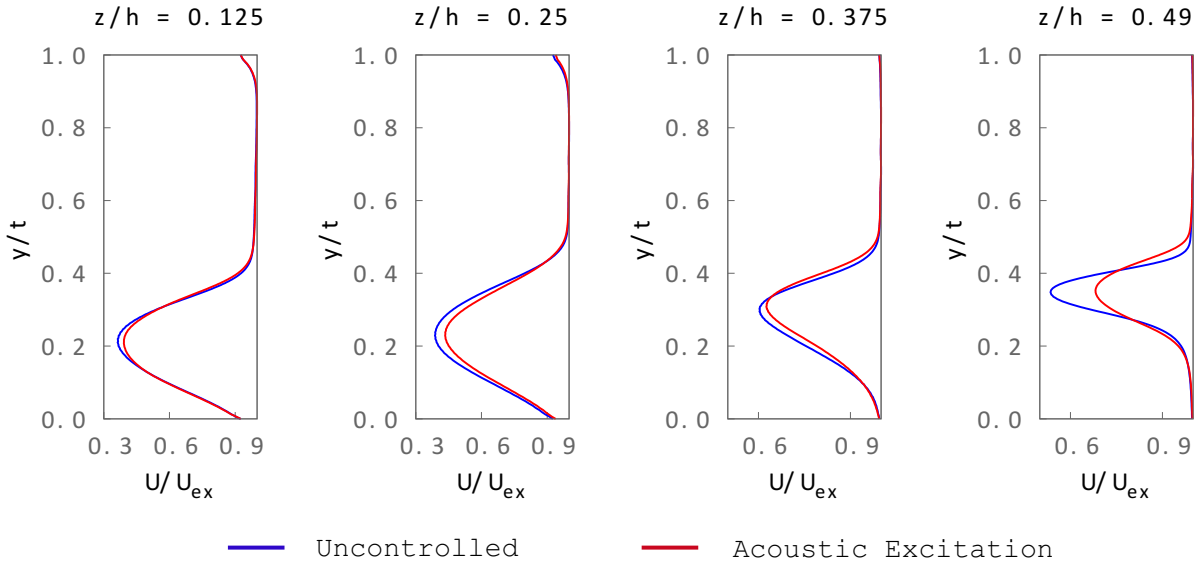

Fig. 9 Pitchwise velocity profiles at the measurement plane normalised by cascade exit velocity.

Total pressure loss coefficient ζ at the measurement plane is compared for the uncontrolled and excited flows in Fig. 10. A significant reduction in total pressure loss is observed for the entire span of the cascade. The core of the corner separation is weakened at the measurement plane shown with acoustic excitation. Enhanced interactions between the corner vortex and midspan region flow as shown by the evolution of the vortical structures in Fig. 8 results in an improved momentum transfer across the separated shear layer encompassing the corner vortex. This results in reduced losses at the measurement plane shown which is the actual exit of the cascade passage. Therefore, it can be stated that acoustic excitation is effective in reducing the losses in the cascade flow under investigation.

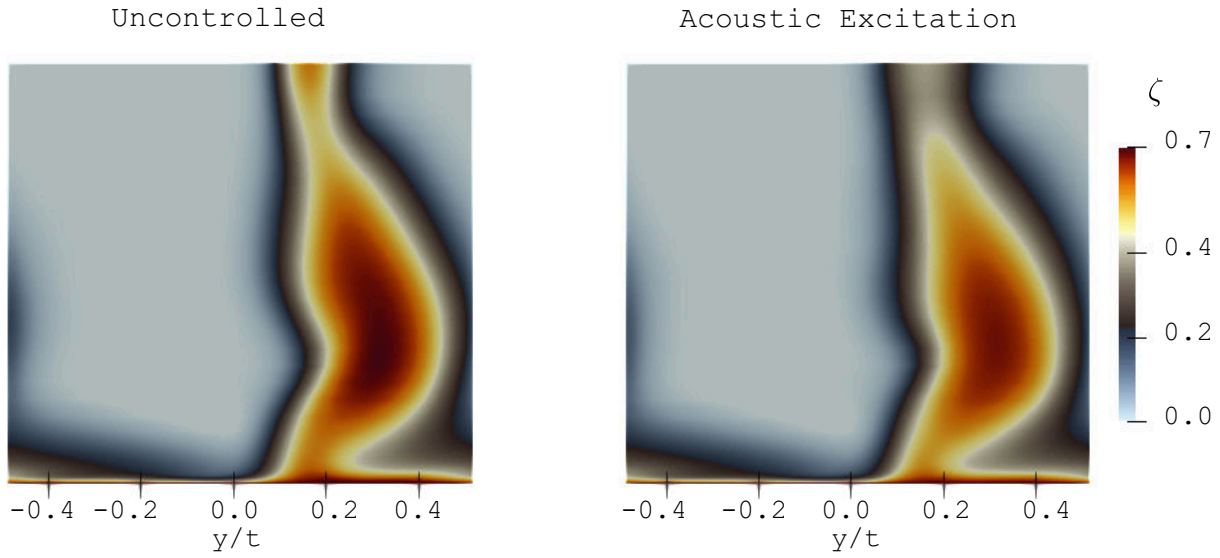

Fig. 10 Total pressure loss coefficient comparison at the measurement plane.

B. Effect of Excitation Parameters

1. Effect of Excitation Frequency

The frequency of sound waves introduced in the uncontrolled flow field for excitation of the flow separation and loss mechanisms is of crucial importance in the effectiveness of acoustic excitation as substantiated by the previous research [7, 9, 10]. It has been investigated previously [7, 9] that acoustic excitation is most effective when applied with the frequency of the most amplified disturbances in the uncontrolled flow. In other words, locking the sound wave frequency to the dominant frequency in the uncontrolled flow results in earlier transition of the separated shear layer to turbulence because amplification of the instabilities and breakdown of shear layer take place earlier compared to baseline flow. This helps improving the momentum transfer across the shear layer and reducing the extent of separation and losses in the flow. Based on this, a range of acoustic excitation frequencies comparable to the dominant frequencies obtained in the uncontrolled flow are utilised in exciting the cascade flow at a constant excitation amplitude, $SPL = 145dB$. The results are compared to the uncontrolled flow in terms of the local total pressure loss coefficient at the measurement plane as illustrated in Fig. 11. The most effective excitation frequency corresponds to $St_c = 2.72$ which reduces the total pressure losses substantially at MP. Excitation with $St_c = 2.18$ also reduces the losses at MP considerably whilst its effectiveness is not comparable to excitation with $St_c = 2.72$. And the third frequency applied, $St_c = 1.36$, has little to no effect on MP losses.

To illustrate the mechanism behind the effectiveness of acoustic excitation, evolution of the corner flow separation is visualized by means of iso-surfaces of Q-criterion at $Q = 10^9$ as shown in Fig. 12. Excitation with $St_c = 1.36$ has no discernable effect on the corner vortex evolution. On the other hand, excitation with $St_c = 2.18$ confines the corner vortex into a narrower region with a reduced strength that results in reduced losses at MP. $St_c = 2.72$ excitation substantially changes the corner vortex topology such that corner vortex covers a wider area in spanwise direction with elongated vortical structures and reduced strength. Therefore, this results in a reduction in the losses through the cascade.

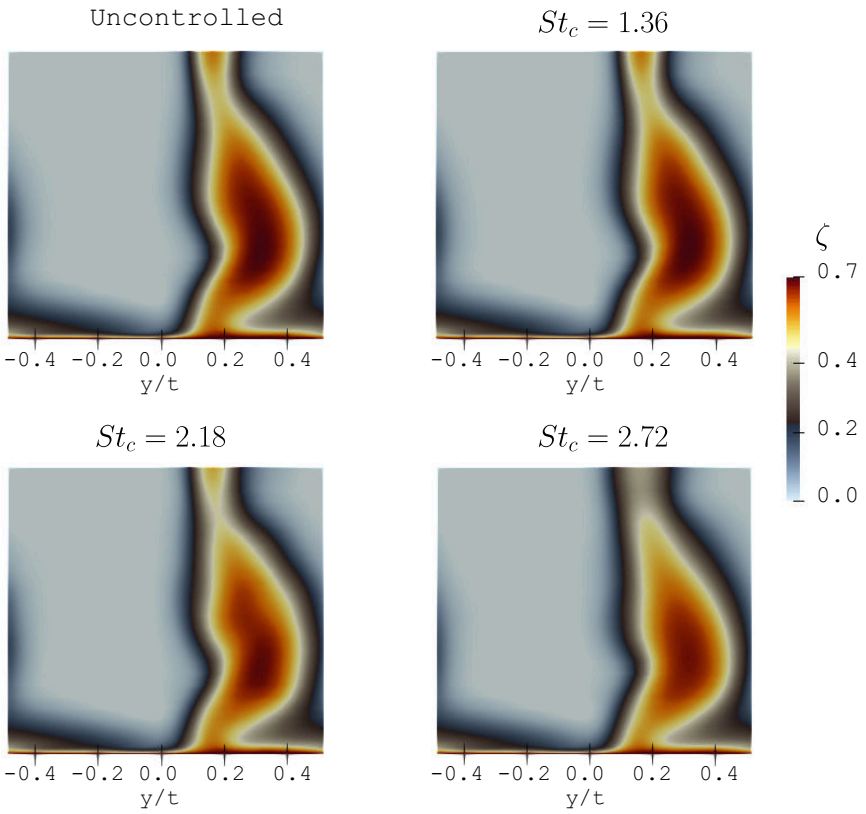

Fig. 11 The effect of acoustic excitation frequency on total pressure loss coefficient distribution at the measurement plane for $SPL = 145dB$.

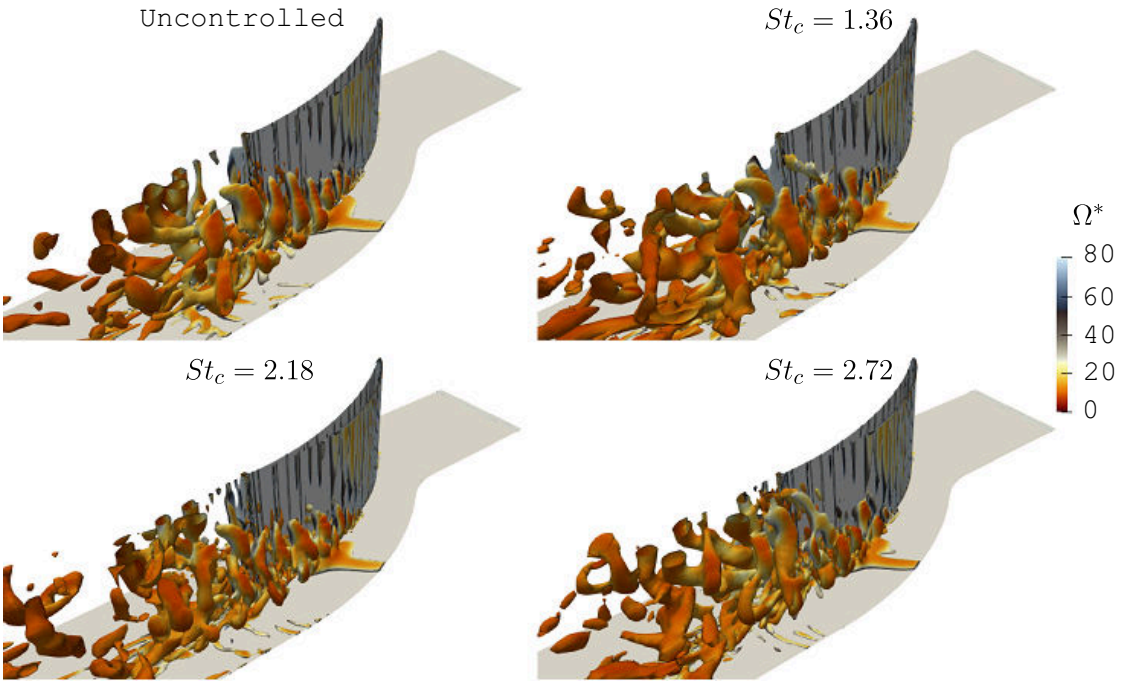

Fig. 12 The effect of excitation frequency on the iso-surfaces of Q-criterion at $Q = 10^9$ coloured by Ω^*.

2. Effect of Excitation Amplitude

The amplitude of sound waves is another fundamental parameter on the effectiveness of acoustic excitation. Therefore, the focus of this section is a parametric study on the excitation amplitude at the most effective frequency obtained in the previous section, i.e., $St_c = 2.72$. The range of excitation amplitudes under consideration are $SPL = 131dB$, $145dB$ and $151dB$ at the inlet boundary of the computational domain. The effect of excitation amplitude is illustrated in terms of the change in total pressure loss coefficient at MP in Fig. 13. It is observed that even the smallest amplitude under investigation $SPL = 131dB$ reduces the losses in the LCC passage considerably with the main effect being at the core of the corner separation. Increasing the excitation amplitude to $SPL = 145dB$ results in further reduction in the losses at MP as such a substantial reduction in the corner separation losses is obtained. The highest excitation amplitude under investigation, on the other hand, has no considerable improvement compared to excitation with $SPL = 145dB$. Furthermore, a threshold excitation amplitude at $SPL = 145dB$ is observed beyond which the ability of acoustic excitation to decrease the extent of flow separation becomes degenerate and eventually no further improvement is observed with a further increase in the amplitude.

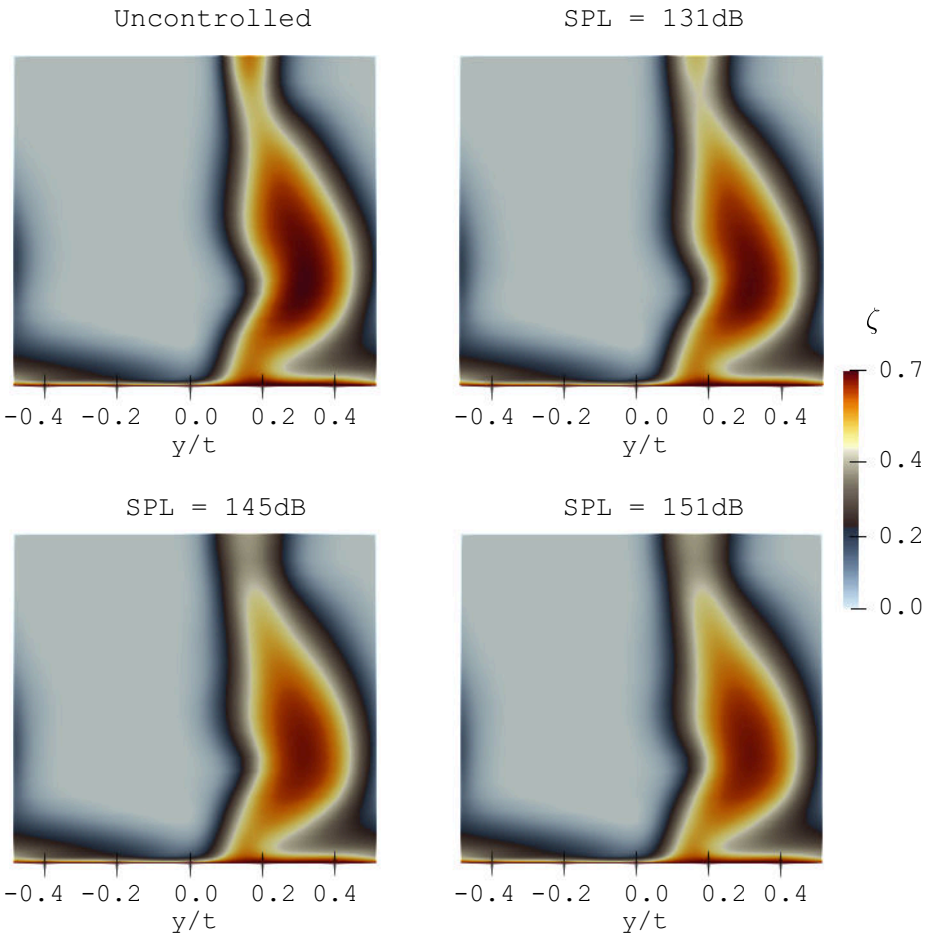

Fig. 13 The effect of acoustic excitation amplitude on total pressure loss coefficient distribution at the measurement plane at $St_c = 2.72$.

The physical mechanism behind the enhanced effectiveness of acoustic excitation with increasing sound wave amplitude is investigated by visualization of the vortical structures as demonstrated in Fig. 14. Excitation of the baseline flow with sound amplitude $SPL = 131dB$ alters the evolution of corner vortex in a way that the coherence of the corner vortex is broken down resulting in larger vortices that extend in the spanwise direction and interact with the midspan, undisturbed flow to enhance the momentum transfer between the corner separation and undisturbed flow around the corner separation. The improvement in the momentum transfer across the separated shear layer encompassing the

corner vortex reduces the pressure losses downstream of the LCC passage. Increase in the excitation amplitude results in further break down of the corner vortex with further elongation of the vortical structures that enhance the momentum transfer. As a result of this process, passage losses are reduced considerably.

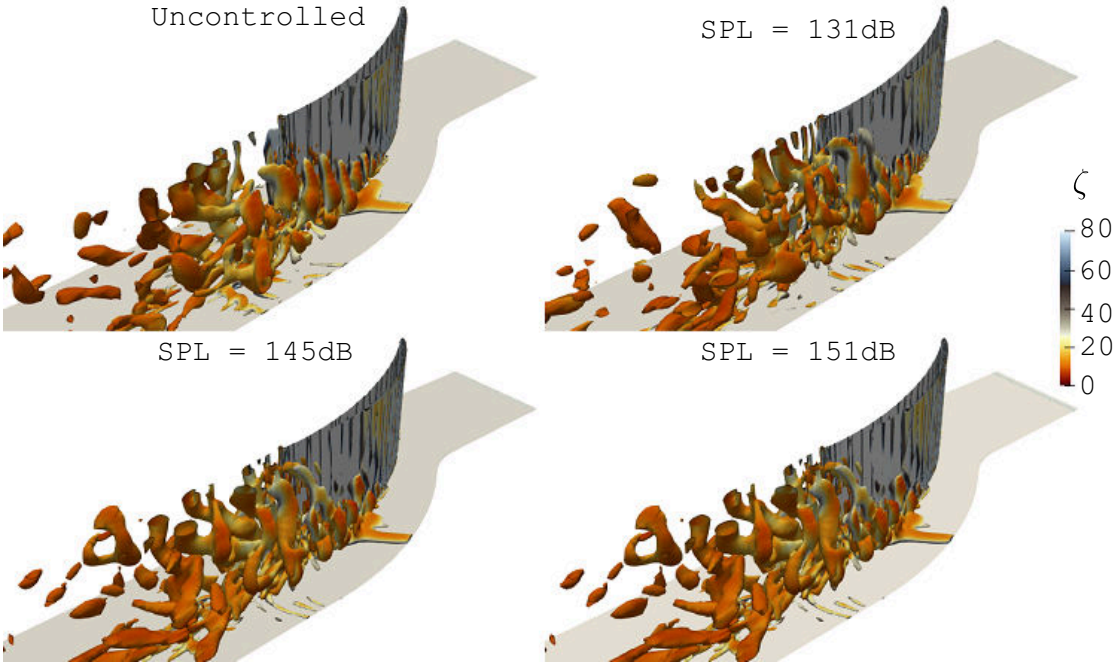

Fig. 14 The effect of excitation amplitude on the iso-surfaces of Q-criterion at $Q = 10^9$ coloured by Ω^*.

V. Conclusions

Numerical modelling of flow separation control through acoustic excitation over a NACA65-K48 linear compressor cascade operating at $Re_c = 560\,x10^3$ and $Ma_1 = 0.67$ is conducted at the aerodynamic design point of the cascade. Improved Delayed Detached Eddy Simulation (IDDES) is used in modelling both the uncontrolled and excited flows. It has been shown that the IDDES model can reasonably capture the unsteady characteristics as well as turbulent scales in the uncontrolled flow field, which is dominated by secondary flows such as corner separation. Therefore, it is suitable for flow control applications including acoustic excitation.

The main focus of this study is the investigation of the effects of acoustic excitation frequency and amplitude on flow separation over NACA65-K48 cascade. It has been observed that acoustic excitation can significantly suppress flow separation when applied under certain excitation parameters, i.e., excitation frequency and amplitude. The effective excitation frequency has been obtained as the frequency of the most amplified disturbances in the uncontrolled flow field. Excitation with the dominant frequency of the baseline flow promotes the flow separation suppression for a range of excitation amplitudes. An improvement trend is observed on the pressure losses with increasing excitation amplitude although there is a threshold excitation amplitude at $SPL = 145dB$ for acoustic excitation to be effective. Beyond this amplitude, little to no improvement is gained with a further increase on the sound wave amplitude.

It has been shown in the present work that the effect of acoustic excitation on flow separation over a NACA65-K48 cascade geometry at aerodynamic design point can be predicted by using IDDES method. It is anticipated that current study can propose a new approach on the control of secondary flows by means of sound excitation that can help improve the three-dimensional design and performance of high-speed compressor cascades. More detailed investigations of the effective excitation frequency and amplitude remain as a future work.

Acknowledgments

The authors would like to express their gratitude to Rolls-Royce plc. for permission to publish the paper. This work was supported by the UK Engineering and Physical Sciences Research Council (EPSRC) grant EP/S513842/1.

References

[1] Zambonini, G., Ottavy, X., and Kriegseis, J., "Corner Separation Dynamics in a Linear Compressor Cascade," *Journal of Fluids Engineering*, Vol. 139, No. 6, 2017. https://doi.org/10.1115/1.4035876, 061101.

[2] Dong, Y., Gallimore, S. J., and Hodson, H. P., "Three-Dimensional Flows and Loss Reduction in Axial Compressors," *Journal of Turbomachinery, Transactions of the ASME*, Vol. 109, No. 3, 1987, pp. 354–361. https://doi.org/10.1115/86-GT-193.

[3] Saito, S., Yamada, K., Furukawa, M., Watanabe, K., Matsuoka, A., and Niwa, N., "Flow Structure and Unsteady Behavior of Hub-Corner Separation in a Stator Cascade of a Multi-Stage Transonic Axial Compressor," Oslo, Norway, 2018. https://doi.org/10.1115/GT2018-76480, v02AT39A030.

[4] Schulz, H. D., Gallus, H. E., and Lakshminarayana, B., "Three-Dimensional Separated Flow Field in the Endwall Region of an Annular Compressor Cascade in the Presence of Rotor-Stator Interaction Part II: Unsteady Flow and Pressure Field," *Journal of Turbomachinery, Transactions of the ASME*, Vol. 112, No. 4, 1990, pp. 669–688. https://doi.org/10.1115/89-GT-77.

[5] Yarusevych, S., Sullivan, P. E., and Kawall, J. G., "Effect of acoustic excitation amplitude on airfoil boundary layer and wake development," *AIAA Journal*, Vol. 45, No. 4, 2007, pp. 760 – 771. https://doi.org/https://doi.org/10.2514/1.25439.

[6] Zaman, K. B. M. Q., "Effect of Acoustic Excitation on Stalled Flows Over an Airfoil," *AIAA Journal*, Vol. 30, No. 6, 1992, pp. 1492 – 1499. https://doi.org/https://doi.org/10.2514/3.11092.

[7] Zaman, K. B. M. Q., and McKinzie, D. J., "Control of Laminar Separation over Airfoils by Acoustic Excitation," *AIAA Journal*, Vol. 29, No. 7, 1991, pp. 1075 – 1083. https://doi.org/https://doi.org/10.2514/6.1989-565.

[8] Zaman, K. B. M. Q., Bar-Sever, A., and Mangalam, S. M., "Effect of Acoustic Excitation on the Flow over a Low-Re Airfoil," *Journal of Fluid Mechanics*, Vol. 182, 1987, pp. 127 – 148. https://doi.org/https://doi.org/10.1017/S0022112087002271.

[9] Hsiao, F. B., Jih, J. J., and Shyu, R. N., "The Effect ofAcoustics on Flow Passing a High-AOA Airfoil," *Journal of Sound and Vibration*, Vol. 199, No. 2, 1997, pp. 177 – 178. https://doi.org/https://doi.org/10.1006/jsvi.1996.0618.

[10] Coskun, S., Pachidis, V., Ubulom, I., and Bacic, M., "Improved Delayed Detached Eddy Simulations Applied to a NACA0015 Aerofoil Subject to Acoustic Excitation," *AIAA Aviation Forum 2022*, AIAA Aviation Forum, Chicago, IL, 2022. https://doi.org/https://doi.org/10.2514/6.2022-3237.

[11] Bons, J., Benton, S., Bernardini, C., and Bloxham, M., "Active flow control for low-pressure turbines," *AIAA Journal*, Vol. 56, No. 7, 2018, pp. 2687–2698. https://doi.org/10.2514/1.J056697.

[12] Bernardini, C., Benton, S. I., and Jeffrey, P. B., "The effect of acoustic excitation on boundary layer separation of a highly loaded LPT blade," *Journal of Turbomachinery*, Vol. 135, 2013. https://doi.org/10.1115/1.4007834.

[13] Bernardini, C., Benton, S. I., and Bons, J. P., "Separation control by acoustic excitation on highly loaded low pressure turbine blades," *10th European Conference on Turbomachinery Fluid Dynamics and Thermodynamics, ETC 2013*, 2013.

[14] Bernardini, C., Benton, S. I., Chen, J. P., and Bons, J. P., "Exploitation of subharmonics for separated shear layer control on a high-lift low-pressure turbine using acoustic forcing," *Journal of Turbomachinery*, Vol. 136, No. 5, 2014. https://doi.org/10.1115/1.4025586.

[15] Collins, F. G., and Zelenevitz, J., "Influence of sound upon separated flow over wings," *AIAA Journal*, Vol. 13, No. 3, 1975, pp. 408–410. https://doi.org/10.2514/3.49717.

[16] Spalart, P. R., "Detached-Eddy Simulation," *Annual Review of Fluid Mechanics*, Vol. 41, No. 1, 2009, pp. 181–202. https://doi.org/http://dx.doi.org/10.1146/annurev.fluid.010908.165130.

[17] Shur, M. L., Spalart, P. R., Strelets, M. K., and Travin, A. K., "A hybrid RANS-LES approach with delayed-DES and wall-modelled LES capabilities," *International Journal of Heat and Fluid Flow*, Vol. 29, No. 6, 2008, pp. 1638–1649. https://doi.org/https://doi.org/10.1016/j.ijheatfluidflow.2008.07.001.

[18] Gritskevich, M. S., Garbaruk, A. V., Schütze, J., and Menter, F. R., "Development of DDES and IDDES formulations for the k-ω shear stress transport model," *Flow, Turbulence and Combustion*, Vol. 88, No. 3, 2012, pp. 431–449. https://doi.org/10.1007/s10494-011-9378-4.

[19] Menter, F. R., "Two-equation eddy-viscosity turbulence models for engineering applications," *AIAA Journal*, Vol. 32, No. 8, 1994, pp. 1598–1605. https://doi.org/10.2514/3.12149.

[20] Chen, P. P., Qiao, W. Y., Liesner, K., and Meyer, R., "Location effect of boundary layer suction on compressor hub-corner separation," *Proceedings of the ASME Turbo Expo*, Vol. 2A, No. July, 2014. https://doi.org/10.1115/GT2014-25043.

[21] Eriksson, S., and Nordstrom, J., "Exact Non-reflecting Boundary Conditions Revisited: Well-Posedness and Stability," *Foundations of Computational Mathematics*, Vol. 17, No. 4, 2017, pp. 957–986. https://doi.org/10.1007/s10208-016-9310-3.

[22] Zaabar, K., "Non-reflective Boundary Conditions for Prediction of Acoustic Tones in Non-uniform Mean Flow for Ducted Flows," Ph.D. thesis, University of Southampton, United Kingdom, 2022.

[23] ANSYS, "Fluent 19.1 Theory Guide," Tech. rep., ANSYS, Inc., 2018.

2023-06-08

Control of flow separation in a high-speed compressor cascade through acoustic excitation

Coskun, Seyfettin

AIAA

Coskun S, Rajendran DJ, Pachidis V, Bacic M. (2023) Control of flow separation in a high-speed compressor cascade through acoustic excitation. In: 2023 AIAA Aviation and Aeronautics Forum and Exposition (AIAA AVIATION Forum), 12-16 June 2023, San Diego, USA. Paper number AIAA 2023-3284

https://doi.org/10.2514/6.2023-3284